Model uncertainty in synoptic circulation patterns and precipitation changes in Southern South America using CMIP5 and CMIP6 models

Matias Olmo (✉ molmo@at.fcen.uba.ar)

University of Buenos Aires Faculty of Exact and Natural Sciences: Universidad de Buenos Aires Facultad de Ciencias Exactas y Naturales   https://orcid.org/0000-0003-3324-9040

Maria Laura Bettolli

Universidad de Buenos Aires Facultad de Ciencias Exactas y Naturales

Rocio Balmaceda-Huarte

Universidad de Buenos Aires Facultad de Ciencias Exactas y Naturales

Abstract

The effects of global warming on the regional climate of southern South America (SSA) during the recent decades have been exhaustively documented with consistency throughout the literature. However, the projected changes on temperature- and precipitation-related climate hazards depict an important uncertainty, mostly in the intensity of the changes. This work assessed a set of CMIP5 and CMIP6 global climate models (GCMs) in reproducing the observed atmospheric circulation patterns (CPs) over SSA and their expected changes for the 21st century. Furthermore, the attribution of the seasonal precipitation changes to changes in the CPs was explored for the late future (2070–2100). GCMs were generally able to represent the variety of CPs and their seasonal frequencies, although presenting more deficiencies in capturing their respective precipitation patterns over SSA. Larger model agreement was found in the increasing and/or decreasing frequency of specific CPs for the near future (2040–2070) than for the late future, when model spread became more noticeable. Particularly, CPs associated with larger positive rainfall anomalies over southeastern South America -a hotspot for precipitation extremes- are expected to become more frequent in the near future, whereas their changes in the longer-term are more uncertain. When performing an attributional study, precipitation changes showed important differences between GCMs and were often associated with changes in the intra-pattern variability rather than in the CPs changing frequency. In this way, the modification of the precipitation regime of SSA may not be explained only by changes in the large-scale circulation but probably also by other regional-to-local features.

1. Introduction

During the recent decades, Southern South America (SSA, roughly between 52-74°W and 22-57°S) has experienced the impact of global warming in several regional climatic features including an intensification of extreme weather conditions such as record-breaking temperatures, persistent heatwaves and droughts and heavy storms. These climate hazards lead to multiple socio-economic and environmental impacts (IPCC 2021).

SSA rainfall is modulated by both large- and regional-scale forcings. Rainfall in central Chile increases southward from very dry conditions along the Atacama Desert to more than 3000 mm in southern Chile and is usually associated with the passage of mid-latitude cold fronts in the cold season (April to September) (Quintana and Aceituno 2012). Eastward from the Andes, the northwestern portion of Argentina and Argentinian Patagonia have much drier conditions, mainly due to the topographic blocking effect of the Andes mountains on the extratropical disturbances embedded in the mid-latitude westerlies. Conversely, southeastern South America (SESA) has a uniform rainfall annual cycle with large amounts of precipitation, frequently caused by extreme events. They are typically associated with extratropical synoptic systems during the cold season, cyclogenesis during the transition seasons and mesoscale convective systems in the warm season (October–March) (Cavalcanti 2012). Other forcings can be mentioned, such as the role of the Atlantic and Pacific oceans: sea surface temperature (SST) anomalies in the equatorial Pacific and western Indian Ocean -related to El Niño–Southern Oscillation (ENSO)- induce circulation anomalies that promote heavy rainfall over SESA especially during spring (Robledo et

al. 2013). Moreover, positive SST anomalies over the southwestern Atlantic basin together with a weak activity of the South Atlantic Convergence Zone (SACZ) are linked with positive rainfall anomalies during summer (Doyle and Barros 2002). Another key ingredient favouring extreme rainfall over SESA is the availability of heat and moisture from the South American Low Level Jet (SALLJ), advecting warm and humid air from the Amazonas (Salio et al. 2007; Penalba and Robledo 2010).

In terms of long-term variability, upward precipitation trends have been observed over southeastern South America -SESA, covering northeastern Argentina, southern Brazil and Uruguay- while downward trends were detected in central and southern Chile (Olmo et al. 2020). Although the observed changes are expected to intensify during the 21st century, the confidence in future precipitation patterns varies among regions and on the spatio-temporal resolution of the climate modelling experiment employed for the projections (Almazroui et al. 2021; Blázquez and Solman 2020; Diaz et al. 2020; Olmo et al. 2022). This is due to different challenging aspects of climate modelling, such as the variety of models and parametrizations, emission scenarios and natural variability (Lehner et al. 2020).

The use of global climate models (GCMs) is essential for understanding multiple physical processes involved in the climatic system, as well as for interpreting its long-term past and future changes. The *Coupled Model Intercomparison Project* (CMIP) moves forward in a collaborative experiment designed for these purposes, making multi-model outputs for different scenarios available in a standardised format. However, the dispersion among these simulations is still important and has a strong influence on decision-making and climate adaptation policies under global warming (IPCC 2021). Moreover, despite climate change being human-induced by an exacerbated emission of greenhouse gases to the atmosphere, the attribution of climate change to different mechanisms involved in the climate system can ease our interpretation of the observed and projected changes contributing to the climate modelling research.

Classifications of atmospheric circulation patterns (CPs) can provide useful information in climate variability studies and process-based model evaluations. Particularly, CPs represent a valuable perspective for model assessment on the large-scale physical mechanisms behind the regional and local climate (Prein et al. 2019). This approach has been exhaustively used in the literature, showing its potential in different implementations around the world (Bettolli et al. 2014; Gibson et al. 2016; Schuenemann and Cassano 2010; Faranda et al. 2020; Espinoza et al. 2021). Recently, Olmo and Bettolli (2021) described the main atmospheric features over SSA based on a Self-Organising Maps (SOM) clustering technique of middle-level geopotential height anomalies. The obtained CPs were able to differentiate multiple precipitation patterns related to extreme events over SESA - that is a remarkable hotspot for extreme rainfall events. These CPs were then used in the design of empirical statistical downscaling models (ESD) for precipitation extremes in the region (Olmo et al. 2022). The authors detected an increasing model uncertainty in the ESD precipitation projections over SESA for the late 21st century, partially caused by GCMs spread. ESD strategies make use of the relationship between large-scale predictors and the predictand variable to generate high-resolution outputs based on GCM predictor information (Maraun and Widmann 2018). Thus, evaluating the CPs representation by the GCMs may

help to ascertain our confidence in future precipitation projections. Furthermore, using a weather-typing approach for climate change attribution has been proposed in different studies showing its potential to diagnose changes in different climate regimes (Schuenemann and Cassano 2010; Cahynová and Huth 2016; Olmo et al. 2020; Espinoza et al. 2021; Prein and Mearns 2021). In this way, this is an interesting path to assess GCM performance and disentangle future rainfall changes over SSA that has not been substantially explored yet.

Thereby, the aim of this work is the assessment of a set of CMIP5 and CMIP6 GCMs in simulating the observed CPs identified over SSA in a previous study (Olmo and Bettolli 2021) considering their historical periods: 1979-2005 and 1979-2014, respectively. Furthermore, to analyse their changes in a context of global warming based on the worst-case scenarios in each experiment (RCP8.5 and SSP5-8.5), with the intention of better comprehending model uncertainty in precipitation changes for the 21st century through an attributional analysis.

2. Data and methods

2.1 Data

The GCMs evaluation was based on a SOM classification of 16 CPs constructed in a previous study using daily geopotential height anomalies at 500 hPa (Z500) over SSA (Figure 1a) and observational rainfall from an interpolation of meteorological stations, obtained by a bilinear scheme (Olmo and Bettolli 2021). This precipitation dataset was inter-compared with other precipitation products containing information from different sources and was found to be suitable for describing the precipitation features over SSA.

The SOM clustering technique generates a topologically ordered map of nodes (or CPs) organising the daily input fields by iteratively updating the representative nodes based on a non-linear neural network algorithm (Kohonen, 2001). Details about how this methodology was employed can be found in Olmo and Bettolli (2021). In that study, reference data were taken from the *European Centre for Medium-Range Weather Forecast* ERA-Interim reanalysis during 1979-2017 (Dee et al. 2011). Here, in the case of the model simulations, Z500 anomalies were estimated for a set of 6 CMIP5 and 6 CMIP6 GCMs listed in Table 1 (Taylor et al. 2012; Eyring et al. 2016) during their historical periods (1979-2005 and 1979-2014, respectively) and the projections for the 21st century under the worst-case scenario in each experiment (RCP8.5 and SSP5-8.5, respectively). This was done by subtracting the Z500 daily annual cycle in each grid point considering the historical period of each CMIP experiment as reference. For comparison purposes, all GCMs were regridded to a common grid of 2° using a bilinear scheme. Additionally, we used GCMs precipitation outputs during the historical and future periods re-gridded to a common grid of 2° through bilinear interpolation for comparison purposes.

Table 1 List of GCMs from the CMIP5 and CMIP6 experiments used in this study.

Model name	Experiments	Resolution	Institute	Reference
CanESM2	CMIP5 historical (1979-2005) and RCP8.5 (2041-2100) (r1i1p1 run)	2.8° × 2.8°	Canadian Centre for Climate Modelling and Analysis, Canada	Kirchmeier-Young et al. 2017
CMCC-CMS		1.9° x 1.9°	Centro Euro-Mediterraneo per I Cambiamenti Climatici, Italy	Fogli et al. 2009
CNRM-CM5		1.4° × 1.4°	Centre National de Recherches Meteorologiques/ Centre Europeen de Recherches et de Formation Avancee en Calcul Scientifique, France	Voldoire et al. 2011
MPI-ESM-LR		1.9° × 1.9°	Max Planck Institute for Meteorology, Germany	Giorgetta et al. 2013
MPI-ESM-MR		1.9° × 1.9°		
NorESM1-M		1.9° × 2.5°	Norwegian Climate Centre, Norway	Bentsen et al. 2013
CanESM5	CMIP6 historical (1979-2014) and SSP585 (2041-2100) (r1i1p1f1 run)	2.8° × 2.8°	Canadian Centre for Climate Modelling and Analysis, Canada	Swart et al. 2019
INM-CM5-0		1.5° × 2.0°	Russian Institute for Numerical Mathematics, Russia	Volodin et al. (2017)
MPI-ESM2-1-HR		0.9° × 0.9°	Max Planck Institute for Meteorology, Germany	Mueller et al. (2018)
MPI-ESM2-1-LR		1.9° × 1.9°		
NorESM2-LM		1.9° × 2.5°	Norwegian Climate Centre, Norway	Bentsen et al. 2013
NorESM2-MM		0.9° x 1.2°		

2.2 Methods

CPs evaluation

First, the simulated daily Z500 anomalies fields were projected into the reanalysis-based SOM based on the Euclidean distance to each CP centroid, so each GCM daily field is assigned to one of the sixteen CPs presented in the SOM. Additionally, the general warming of the atmosphere causes an elevation of the geopotential levels due to thermal expansion, which is why Z500 presents an upward trend in a climate change scenario (Maraun and Widmann 2018). In order to project the future Z500 anomalies fields to the SOM, this trend was filtered prior to the CP assignment. Since the removed trend corresponds to a shift of Z500 mostly caused by global warming, the resulting anomalies indicate changes mainly due to dynamical atmospheric changes (Faranda et al. 2020). Furthermore, the accuracy of the assignment of the GCMs daily fields to the reference (ERA-Interim) SOM nodes -usually called model projection onto the cluster centroid- was quantified through a quantization error, that is calculated as the average Euclidean distance between the input daily fields and the reference dataset (Quagraine et al. 2020). This error can tell whether the simulated fields are within the reanalysis catalogue of Z500 configurations.

The representation of the CPs was assessed based on their seasonal frequency for each GCM, considering the warm and cold austral seasons (October to March and April to September, respectively). This was replicated for the historical period of each CMIP experiment and for the near and late-future periods (2040-2070 and 2071-2100, respectively).

For the historical period, precipitation anomalies were constructed for each CP in the reference observational dataset and the GCMs using the common reference period 1986-2005. Their significance was tested by means of a student's t-Test with the alternative hypothesis that the true difference in means is not equal to zero (the difference between the climatological mean and the conditional mean to the occurrence of a CP, as expressed by the corresponding anomalies values), with a confidence level of 95% (Wilks 2019). Model performance in reproducing those spatial patterns was synthesised through heatmaps and Taylor diagrams (Taylor 2001). These diagrams quantify the degree of statistical similarity between the reanalysis dataset and the different GCMs, showing the Spearman correlation coefficient, the normalised standard deviation and the centred root mean squared error. Statistical significance was analysed by means of a Spearman correlation test (between two samples) and a two-sided F-test for the comparison of the modelled and observed spatial variance (in the case of the standard deviation) (Wilks 2019).

Attribution method

Precipitation changes in the late future as depicted by the set of GCMs were analysed through the attribution method developed in Schuenemann and Cassano (2010), performing a linear decomposition of the rainfall changes based on precipitation and CPs frequencies and intensities. Similar procedures were considered in the literature to interpret future climate changes in different regions, highlighting the potential of a CPs approach (Cassano et al. 2007; Cattiaux et al. 2013, Cahynová and Huth 2016). For

clarity, a similar explanation to the one shown by Schuenemann and Cassano (2010) is presented here. One can account for precipitation changes due to changes in atmospheric circulation by analysing the frequency of each CP, starting from equation 1:

$$PP = \sum_{(i=1)}^{CP} f_i\, p_i \quad (1)$$

Here, the total precipitation at a grid cell (PP) can be obtained by adding up the contribution of each CP_i, which can be obtained as the product between the frequency of the CP (f_i) and the average daily precipitation during those days with CP_i (p_i). This procedure can be disentangled for the warm and cold seasons, separately, and can be replicated for any climatological period of interest, like the reference period 1986-2005 and the late-future period 2071-2100. Moreover, future precipitation changes can be attributed to changes in CPs frequency () and to changes in precipitation intensities when occurring specific CPs (). In this way, the future precipitation can be expressed as:

$$PP_{future} = \sum_{(i=1)}^{CP} (f_i + \Delta f_i)(p_i + \Delta p_i) \quad (2)$$
$$PP_{future} = \sum_{(i=1)}^{CP}(f_i.p_i + f_i.\Delta p_i + \Delta f_i.p_i + \Delta f_i.\Delta p_i) \quad (3)$$

In equation (3), the first term corresponds to the precipitation in the reference historical period. The second term represents future changes only due to changes in daily rainfall intensities - whereas the CP frequency remains the same - and is referred to as *intrapattern variability component*. These changes include thermodynamic processes occurring when a specific CP takes place that may change precipitation amounts, such as water vapour availability and evaporation processes. The third term is referred to as *pattern frequency change* and reflects changes that happen due to a changing frequency of CPs in the future, keeping the related daily precipitation amounts as they were in the past. Hence, this term is explained by some CPs occurring more and others less frequently, associated with changes in atmospheric circulation. The fourth and last term is due to changes in CPs frequency acting on rainfall changes, which is referred to as the *combined component*, usually a residual term with smaller magnitude than the other terms.

In the present study, this method was used to assess future rainfall changes over SSA for 2071-2100 with respect to 1986-2005, considering the warm and cold seasons, separately. The procedure was done individually for each GCM and a model ensemble for each CMIP experiment was estimated for the sake of conciseness. Furthermore, model uncertainty was addressed by a signal-to-noise analysis: following Coppola et al. (2021), the average change of the model ensemble was compared to the standard deviation computed within each ensemble member (that is, each GCM). If the absolute value of the ratio between the average change and the standard deviation is greater than one, then these changes are *robust* and can be considered different from the noise associated with intermodel variability.

3. Results

3.1 GCMs capability in the historical period

The dominant atmospheric configurations over SSA presented in Figure 1a depict the 16 CPs of Z500 anomalies identified by Olmo and Bettolli (2021) through a SOM clustering. The CPs are topologically ordered in the SOM, with the corner patterns representing CPs that differ the most from each other. The CPs presented positive and negative structures that disturb the typical westerly flow of mid-latitudes. In the bottom SOM, anticyclonic centres (positive anomalies) mostly cover the domain, producing an upper-level ridge often centred in the southern Atlantic Ocean. In the middle-right SOM, negative Z500 anomalies were mainly observed in the Atlantic Ocean, with different intensity and location among CPs. When analysing the top-right SOM, wide negative centres positioned over the Atlantic Ocean entered the continent, while positive anomalies were located in the southern Pacific Ocean. In the case of the top-left SOM, an anomalous cyclonic centre affected the southern Pacific Ocean and southern tip of South America and an anticyclonic centre positioned over the Atlantic Ocean. This structure of negative anomalies over the Pacific Ocean allows the intrusion of cold and humid air from the south-west to southern Chile, while the positive anomalies in the Atlantic Ocean favours warmer and humid air from lower latitudes east of the Andes.

The spatial patterns of rainfall anomalies associated with each CP are illustrated in Figure 1b for the warm and cold seasons (left and right panels, respectively). The variety of configurations at the middle-level atmosphere represented in the SOM were able to differentiate precipitation structures in different areas of the domain. During the warm season, CPs in the top of the SOM enhanced rainfall over sectorised areas of SSA, from central Argentina to southern Brazil (from left to right in the SOM), following the shift of the Z500 structures to the east. In a previous study, these CPs were found to statistically enhance the occurrence of extreme rainfall events in areas like SESA (Olmo and Bettolli 2021). Whereas CPs at the bottom SOM typically depicted negative rainfall anomalies over SESA and positive anomalies in central and southern Argentina. West of the Andes, CP14 and CP13 were related to larger precipitation amounts in central and southern Chile, while CPs in the middle SOM tended to show negative rainfall anomalies over the region. During the cold season, negative anomalies were more predominant throughout most of SSA for the CPs at the top SOM - related to this season being drier in central SSA - and enhanced precipitation was seen for the bottom-right CPs.

In terms of model evaluation, the quantization errors when projecting the Z500 GCMs fields were first estimated for the historical and are available in Table S1 (see Supplementary Material). The errors found for the historical simulations were, in most cases, of the same order or less than those found for the reanalysis, so the synoptic patterns simulated by the GCMs were typically included within the ERA-Interim reanalysis data space. Only CNRM-CM5 and INMCM5 presented average quantization errors larger than in the reanalysis, but close to them anyways. The representation of this classification of CPs by the selected GCMs was then evaluated by studying the frequency of days distributed within the SOM in each model (Figure 2a). GCMs were generally able to capture the distribution of days for each CP as depicted by ERA-Interim, with larger frequencies at the bottom-right (as CP4) and top-left CPs (as CP13) in the SOM during both seasons of the year, between 9% and 11% of days in each case, although CPs located at the top-right SOM also showed high frequencies during the cold season. Models tended to underestimate the maximum frequencies in CP4 and CP13 for the warm and cold seasons, respectively, such as MPI-

ESM-LR and CNRM-CM5. Other structures like CP9 and CP11 were usually overestimated, especially during the warm season. Note that, following the topological order of the SOM, the underestimations of specific patterns were typically balanced by overestimations of the neighbour nodes (and the other way around). This is due to models not capturing the exact differences between similar nodes, at least not in the way the ERA-Interim reanalysis depicts them.

Furthermore, the correspondence in this representation was quantified based on correlations between the CPs frequencies of ERA-Interim and each GCM (Figure 2b). Note that these correlation values are only taken as indicators of how well the models reproduce the frequency distribution among the SOM and are not considered as a robust statistical measure. Relatively high correlation values were found, usually between 0.5 and 0.75. No distinctive behaviour was detected between CMIP experiments or between seasons of the year, although the patterns at the top of the SOM showed significant correlations for most of the GCMs in the warm season (CP14-16), while the same was found for the patterns at the bottom of the SOM during the cold season (CP2-4). The lowest correlations were found in the CMCC-CMS and MPI-ESM-LR models during the warm season, while the highest correlations were found for NorESM1-M and CanESM5, always significant and of 0.76 and 0.73 in the cold and warm seasons, respectively.

In the following step, models were assessed in terms of how well they simulated the rainfall patterns over SSA associated with each CP. The analysis of these spatial patterns was synthesised through Taylor diagrams for the nodes at the corners of the SOM (CP1, CP4, CP13 and CP16 in Figure 3a) showing one point for each model and one square for each CMIP experiment ensemble. The spatial correlation and normalised standard deviation (SD) values depicted in these diagrams but for all the CPs were also illustrated as heatmaps (Figure 3b). Models underestimated the spatial variability of rainfall anomalies in SSA (since the cloud of points was always below the line of 1 SD) and generally presented low-to-medium correlations, although some models reached values of around 0.8 like NorESM2-LM in CP16 in the warm season. No clear differences were identified between seasons and CMIP experiments, although the Norwegian GCMs NorESM1-M from CMIP5 and NorESM2-LM and NorESM2-MM from CMIP6 typically showed the highest correlation values among CPs (significant in most of the cases). In terms of SD, CanESM2 (NorESM2-MM) exhibited the smallest differences with the reference dataset for the warm (cold) season, while CP9 was the most underestimated during the warm season. CMIP6 models seemed to show less intensity differences in the CP structures, as they were found to be more significantly similar to the observations in terms of their spatial variance (marked with asterisks in the heatmap). In addition, the maps for CMIP5 and CMIP6 ensembles were illustrated in Figure S1 (Supplementary Material). As presented in the Taylor diagrams of Figure 3a, they showed large underestimations of the spatial variability -with reduced rainfall values over all the domain- probably due to these patterns being constructed as the average of the individual model anomalies. This strengthens the importance of assessing models individually and is valuable information for understanding model projections of rainfall as will be discussed later in the attributional analysis.

Thus, the different GCMs were able to identify the link between large-scale circulation and precipitation variability over SSA, although showing some limitations in reproducing the correct structures of rainfall

anomalies and often differing among them as measured by the metrics analysed here.

3.2 CPs future projections

In a global warming scenario, atmospheric circulation may present dynamic and thermodynamic changes at a regional scale that can modulate precipitation variability and intensities. It is well known that large-scale variables -such as geopotential height and winds in the mid-level atmosphere- are generally better represented in GCMs than surface variables (Maraun and Widmann 2018), which is the motivation behind assessing precipitation changes and model spread based on a weather-typing approach. In this line, the temporal evolution of CPs frequencies for the near and late future periods (2041-2070 and 2071-2100, respectively) was analysed in terms of the percentage of change compared to the reference period 1986-2005 (Figures 4 and 5).

The quantization errors for the late-future period (2070-2100) are available in Table S1 (see Supplementary Material). As shown in the previous section, the errors found for the historical period were similar among GCMs and reanalysis. Furthermore, these errors were generally of similar value during the future scenarios, indicating an acceptable extrapolation of the reanalysis-trained classification of CPs for the late 21st century.

In the near future (Figure 4), CPs in the top row SOM -such as CP15 and CP16, depicting a dipolar structure of Z500 anomalies leading to a mid-level trough propagating to the east- are expected to become more frequent during the warm season, which is consistent among most of the GCMs from both CMIP5 and CMIP6 experiments used in this study. In these CPs, models presented more differences in the intensity of the changes, with changes near 15% in most of the simulations but up to 30% in MPI-ESM-LR. CPs in the bottom-left SOM generally showed reduced frequencies -like CP1 and CP2- in most of the GCMs, while the rest of the patterns in the SOM (such as CP7 and CP11) did not present clear and congruent changes among models. During the cold season, the frequency of CPs in the near future is more similar to the historical period than in the warm season. Changes in CPs frequency were more pronounced for CP2 and CP7 showing increases in many of the selected GCMs, particularly from the CMIP5 experiment. Moreover, CPs in the top of the SOM showed slight diminutions -larger for CP15 and CP16- mostly for the CMIP5 simulations.

In the late future (Figure 5), a reduced agreement was found among GCMs, both in the sign and the intensities of the changes in CPs frequencies, mostly during the warm season. For instance, the CPs located in the top SOM that presented increases for the near future (CP15 and CP12) show the largest number of models agreeing in the upward (downward) trends in the CP frequency, but notably differing in the magnitude of the change. However, most of the CMIP6 models showed reductions in their frequency, especially in CP16. Reductions were also found for CP12, but with larger agreement among simulations, which were nearly 30% in most of the cases and up to 50% in CanESM2. CPs at the bottom-left SOM tended to present increases in their frequency such as CP2, which was consistent especially in the CMIP6 experiment. Whereas the rest of the CPs showed both slight positive and negative changes among GCMs, of lower magnitude in CPs like CP4 and CP8. During the cold season, the agreement among models from

both CMIP experiments was clearly larger, with CPs at the bottom-left SOM -depicting positive Z500 anomalies related to anticyclonic structures in most of SSA- presenting large increases compared to the reference period. Other CPs like the ones in the top of SOM, showing both cyclonic and anticyclonic centres of varied intensity and location over SSA, presented a reduction in their frequency that has consistency among GCMs, indicating, for instance, favourable large-scale conditions for less rainfall in some areas of central SSA and SESA during this season. Note, however, that precipitation in those regions could present increases anyway, which may be due to the contribution of other CPs during this season and will be discussed in following lines.

As described in Section 2.2, total precipitation changes for the late-future period (2070-2100) were decomposed into the contribution of changes in intrapattern variability, pattern frequency and a combined component where the larger agreement (or robustness) among GCMs was indicated with dots (Figure 6). Model ensemble was constructed by averaging the changes of individual simulations in each CMIP experiment. Focusing mainly over the continent, mean precipitation is expected to increase (decrease) over most of SSA east of the Andes (central and southern Chile), but particularly over southern SESA and mostly during the warm season. The intensity and robustness of these changes were larger for the CMIP5 set of models, whereas CMIP6 depicted even reductions in rainfall over SESA during the cold season (probably related to the decreasing frequency of structures like CPs in the top of the SOM), but with less agreement among simulations. Recall that models have some difficulties and differences when reproducing the link between the large-scale patterns and rainfall anomalies (as shown in Figure 3 and Figure S1), which may be related to the low agreement in precipitation future changes based on the CPs frequency component. The intrapattern variability component -that is, changes within the CPs themselves- frequently dominated the rainfall changes, as it presented a very similar pattern with the Total change. Recall that this component is due to changing characteristics of the related weather within the patterns (Cahynová and Huth 2016). They could be related to the varying intensity and shape of the systems of the different CPs and to other mechanisms beyond the synoptic scale. On the other hand, the other two components of the decomposition were of about one less order of magnitude and presented less agreement among GCMs. The pattern frequency change was related to a slight increase in rainfall during the warm season over southern SESA, especially in the CMIP5 set that depicted robust changes among the model ensemble. This could be related to the positive changes detected in the CMIP5 simulations for the frequency of patterns in the top of the SOM, such as CP15 and CP16. Whereas CMIP6 ensemble presented a decline in mean precipitation in northeastern SESA and in central and southern Chile during the cold and warm seasons, respectively, in line with results from Figure 5. Over the rest of SSA, sligh positive changes were detected in the cold season, but with no clear agreement among simulations. Note that the contributions from the last term (combined component) usually complemented with the pattern frequency change, partly cancelling each other, which is why the intrapattern variability dominated the future changes.

These results indicated that the expected changes in mean precipitation over SSA as depicted by these GCMs are not mainly due to a changing frequency of the CPs found in the SOM and could probably be related to other regional-to-local phenomena. Furthermore, even though a good agreement was found

between GCMs for the near future -mostly in the sign of the changes- a considerable dispersion among the CPs projections was found by the end of the century. Since the agreement among simulations in the long-term changes of the CPs frequency is not large enough, it becomes difficult to infer robust results regarding the future link between the large-scale patterns and rainfall changes.

4. Discussion and final remarks

The present study aimed to assess a set of 12 GCMs from the CMIP5 and CMIP6 experiments in reproducing a classification of CPs and its relationship with rainfall variability. This work contributes to the still incipient attributional studies on rainfall future projections over southern South America (SSA) by the decomposition of precipitation changes due to i) pattern frequency changes; ii) intrapattern variability changes; iii) residual component. The analyses rely on the reanalysis-based Self-Organizing Maps (SOM) classification of Z500 anomalies generated by Olmo and Bettolli (2021).

The range of atmospheric configurations presented in the SOM depicted positive and negative structures of Z500 anomalies that disturb the typical westerly flow of mid-latitudes. CPs located at the top-right of the SOM showed a shift to the east of the Z500 anomalies, leading to enhanced rainfall in sectorised areas of SESA following this movement of the mid-level structures. These atmospheric configurations were previously associated with enhanced occurrence of extreme precipitation events in SESA (Olmo and Bettolli 2021; Martinez and Solman 2022), which may be largely contributing to the positive mean rainfall anomalies identified here.

During the historical period, GCMs were able to simulate the seasonal frequencies of days assigned to each CP in the SOM, exhibiting more limitations in capturing the spatial structure of rainfall anomalies associated with each of them, like in the case of anomalous anticyclonic Z500 structures. The poor model representation of this link between the large-scale mechanisms and the rainfall anomalies is a limitation when trying to perform an attribution of the future changes based on a classification of CPs.

When analysing the near-future (2041-2070) frequencies of the CPs, larger model agreement was found for the warm season changes than for the cold season, with consistent increases in CPs in the top SOM among GCMs from both CMIP5 and CMIP6 experiments. Based on the link CPs-precipitation studied here, these changes are in line with rainfall increases over SESA, which is a region where the literature indicates positive changes in precipitation accumulations largely related to extreme events (Blázquez and Solman 2020; Díaz et al. 2020; Almazroui et al. 2021; Olmo et al. 2022). Models presented more differences in the intensity of the changes, although for the late-future period (2070-2100) a much-reduced agreement was found among GCMs, both in the sign and the intensities of the changes in CPs frequencies, especially during the warm season. In comparison, model agreement was larger during the cold season, with CPs at the bottom-left SOM -depicting positive Z500 anomalies related to anticyclonic structure- presenting large increases compared to the reference period. Thereby, the increases in these sorts of patterns could be depicting a shift in the winter precipitation regime over SSA.

In order to link the CPs changes with future rainfall in the late-future, an attributional analysis linearly decomposing the future rainfall changes following Schuenemann and Cassano (2010) was performed. It was found that changing internal properties of individual CPs -that is, the intrapattern variability component- dominated the total change compared to the pattern frequency change, which was partly related to: i) increases in the warm-season mean rainfall over southern SESA in the CMIP5 models; ii) decreases over central and southern Chile in the CMIP5 models. Note that, since a considerable dispersion was detected among the CPs projections by the end of the century, it becomes difficult to assert that rainfall changes -like the ones expected for SESA (Olmo et al. 2022)- can be explained by the CPs changing frequency only. This may be due to poor or differentiated representation of the CPs-rainfall link between models and with the observations, affecting the attributional analysis. However, these results could tell that precipitation changes over SSA may not be explained only by changes in the large-scale circulation but probably also by other regional-to-local features, such as water vapour availability and transport, smaller-scale atmospheric interactions and land-use changes. This agrees with multiple studies on CPs attribution in different regions, indicating that the intrapattern variability can be largely influencing the observed and future changes (Nilsen et al. 2014; Fleig et al. 2015; Cahynová and Huth 2016; Seager et al. 2019). Locally, Olmo et al. (2020) that employed a hypothetical-trend attributional method with in-situ observations over SSA. The authors found that, although CPs changing frequency would be responsible for a large portion of the observed warm season warming, rainfall changes are only partially influenced by them. Recently, Herrera-Lorméndez et al. (2023) showed that the long-term changes in precipitation over Europe -such as the summer drying- not only arise from CPs frequency changes but changing characteristics within the patterns often dominate the future projections. In this line, most of the analyses of CPs attribution of climate change agree that the fraction of the climatic trends that can be attributed to the CPs changing frequency is larger and more consistent for temperature than for precipitation, which typically has more heterogeneous and irregular trend patterns (Cahynová and Huth 2009; Schuenemann and Cassano 2010; Stryhal and Huth 2018).

It becomes relevant to mention that even though SESA has been identified as a region with remarkable rainfall changes (IPCC 2021), GCMs trends and projections still have strong discrepancies. This was associated with GCMs internal variability and misrepresentation of different forcings including the tropical Atlantic multi-decadal variability, the stratospheric ozone depletion and the increase in greenhouse-gases concentrations (Diaz et al. 2020; Varuolo-Clarke et al. 2021).

In addition, the use of only one CPs classification may limit the attributional analysis as some methodological choices such as the number of patterns, the domain and variable of study and even the clustering technique can contribute to the uncertainty in the circulation patterns analysis. Furthermore, including both dynamic and thermodynamic variables in the clustering procedure may have a potential additional contribution to study the future changes in the CPs (Prein et al. 2019), and is an attractive path in follow-up experiments over SSA.

Note that the GCMs may present different climate sensibility, that is, models are subject to changes under global warming scenarios. Models with high climate sensibility overstate the global cooling effect due to

clouds and aerosols interactions, whereas less sensible models have been found to be more consistent with observed differences in temperature between the northern and southern hemispheres and, thus, may result in more accurate depictions of projected climate change (Wang et al. 2021). In particular, the model NorESM1-M has been identified as a GCM with low climate sensibility, indicating lower long-term changes in the model output (Giorgi et al. 2012; Olmo et al 2022). Thus, it is important to account for such model behaviour -which can have differentiated performance among regions- as it may affect the outcomes of different attributional studies. Thus, given this sensibility and the dispersion in model performance as found in this work, a larger set of GCMs would be optimal to account for model spread and to ascertain our confidence in future climate scenarios.

Overall, this work highlights that GCMs have skills for simulating the association between large-scale CPs and precipitation over SSA, although some CPs-precipitation links were poorly reproduced. Models have a notable spread -especially in the intensity of the changes- which increases model uncertainty in future projections. Hence, the reproduction of other dynamical forcings such as SST patterns, teleconnection processes and the role of model internal variability should be considered for a deeper insight into GCMs performance, particularly in regions like SSA where rainfall has a strong modulation by climate oscillations like ENSO. Thus, performing a cross-time scales assessment can provide additional information on the interaction between the large and synoptic scales (Muñoz et al. 2017). All of this should be considered to generate plausible climate change scenarios. Follow-up studies should focus on using different CP classifications and other sensibility analysis including different variables and statistical methods for the attributional analysis.

Declarations

Competing Interests

The authors have no relevant interests to disclose.

Authors Contributions

All authors contributed to the study conception and design. Material preparation, data collection and analysis were performed by Matias Ezequiel Olmo, Maria Laura Bettolli and Rocio Balmaceda-Huarte. The first draft of the manuscript was written by Matias Ezequiel Olmo and all authors commented on previous versions of the manuscript. All authors read and approved the final manuscript.

Data Availability

Data derived from this study will be available upon request. The gridded precipitation data was presented in Olmo et al. (2021), considering data provided by the National Weather Services of Argentina, Brazil, Uruguay and the Center for Climate and Resilience Research of Chile. The reference circulation patterns were adapted from Olmo et al. (2021) using the ECMWF ERA-Interim reanalysis available at: https://www.ecmwf.int/en/forecasts/datasets/reanalysis-datasets/era-interim. The different model datasets used in this study are available online.

CMIP5 model outputs: https://esgf-node.llnl.gov/search/cmip5/

CMIP6 model outputs: https://esgf-node.llnl.gov/search/cmip6/

Compliance with Ethical Standards

Not applicable.

References

1. Almazroui, M., Ashfaq, M., Islam, M.N., et al. (2021) Assessment of CMIP6 Performance and Projected Temperature and Precipitation Changes Over South America. Earth Syst Environ 5:155–183. https://doi.org/10.1007/s41748-021-00233-6

2. Bentsen M, Bethke I, Debernard JB, et al. (2013) The Norwegian earth system model, noresm1-m - part 1: description and basic evaluation of the physical cli- mate. Geosci Model Dev 6(3):687–720. https://doi.org/10.5194/ gmd-6-687-2013

3. Bettolli ML, Penalba OC (2014) Synoptic sea level pressure patterns– daily rainfall relationship over the Argentine Pampas in a multi- model simulation. Meteorol Appl 21:376–383. https://doi.org/10. 1002/met.13

4. Blázquez, J., Solman, S. (2020) Multiscale precipitation variability and extremes over South America: analysis of future changes from a set of CORDEX regional climate model simulations. Clim Dyn 55:2089–2106. https://doi.org/10.1007/s00382-020-05370-8

5. Cahynová, M., Huth, R., 2009. Changes of atmospheric circulation in central Europe and their influence on climatic trends in the Czech Republic. Theor. Appl. Climatol. 96,57–68.

6. Cahynová M, Huth R. (2016) Atmospheric circulation influence on climatic trends in Europe: An analysis of circulation type classifications from the COST733 catalogue. International Journal of Climatology, 36(7): 2743–2760. https://doi.org/10.1002/joc.4003.

7. Cassano, J. J., P. Uotila, A. H. Lynch, E. N. Cassano (2007) Predicted changes in synoptic forcing of net precipitation in large Arctic river basins during the 21st century, J. Geophys. Res., 112, G04S49,

doi:10.1029/2006JG000332.

8. Cattiaux J, Douville H, Ribes A, Chauvin F, Plante C. (2013) Towards a better understanding of changes in wintertime cold extremes over Europe: A pilot study with CNRM and IPSL atmospheric models. Climate Dynamics. Springer Verlag, 40(9–10): 2433–2445. https://doi.org/10.1007/s00382-012- 1436-7.

9. Cavalcanti I (2012) Large scale and synoptic features associated with extreme precipitation over South America: a review and case studies for the first decade of the 21st century. Atmos Res 118:27–40

10. Coppola, E., Raffaele, F., Giorgi, F. et al. (2021) Climate hazard indices projections based on CORDEX-CORE, CMIP5 and CMIP6 ensemble. *Climate Dynamics*, *57*(5), 1293–1383. https://doi.org/10.1007/s00382-021-05640-z

11. Dee DP, Uppala SM, Simmons AJ et al. (2011) The ERA-Interim reanalysis: configuration and performance of the data assimilation system, Q. J. Roy. Meteorol. Soc. 137: 553–597. https://doi.org/10.1002/qj.828

12. Díaz, L.B., Saurral, R.I., Vera, C.S. (2020) Assessment of South America summer rainfall climatology and trends in a set of global climate models large ensembles. Int J Climatol. 2020; 1–19. https://doi.org/10.1002/joc.6643

13. Doyle, M., Barros, V., (2002) Midsummer low-level circulation and precipitation in subtropical South America and related sea surface temperature anomalies in the South Atlantic. Journal of Climate, 15, 3394–3410.

14. Espinoza, J.C. Arias, P.A. et al. (2021) Recent changes in the atmospheric circulation patterns during the dry-to wet transition season in south tropical South America (1979–2020): impacts on precipitation and fire season. Journal of Climate 34: 9025-9042. https://doi.org/10.1175/ JCLI-D-21-0303.1

15. Eyring V, Bony S, Meehl GA et al. (2016) Overview of the coupled model Intercomparison project phase 6 (CMIP6) experimental design and organization. Geosci Model Dev 9(5):1937–1958. https://doi.org/10.5194/ gmd-9-1937-2016

16. Faranda, D., Vrac, M., Yiou, P., Jézéquel, A., & Thao, S. (2020) Changes in future synoptic circulation patterns: Consequences for extreme event attribution. *Geophysical Research Letters*, *47*, e2020GL088002. https://doi. org/10.1029/2020GL088002

17. Fleig, A.K., Tallaksen, L.M., James, P., Hisdal, H., Stahl, K., 2015. Attribution of European precipitation and temperature trends to changes in synoptic circulation. Hydrol. Earth Syst. Sci. 19, 3093–3107.

18. Fogli PG, Manzini E, Vichi M, Alessandri A, Patara L, Gualdi S, Scoc- cimarro E, Masina S, Navarra A (2009) INGV-CMCC Carbon: A Carbon Cycle Earth System Model, CMCC online RP0061:http://www.cmcc.it/publications/rp0061-ingv-cmcc-carbon-icc-a-carbon-cycle-earth-system-model

19. Gibson, P.B., Perkins-Kirkpatrick, S.E., Renwick, J.A. (2016) Projected changes in synoptic weather patterns over New Zealand examined through self-organizing maps. Int J Climatol 36:3934–3948.

https://doi.org/10.1002/joc.4604

20. Giorgetta MA, Jungclaus J, Reick CH, et al. (2013) Climate and carbon cycle changes from 1850 to 2100 in mpi-esm simulations for the coupled model intercomparison project phase 5. J Adv Model Earth Syst 5(3):572–597. https:// doi.org/10.1002/jame.20038

21. Giorgi, F., Coppola, E., Solmon, F., Mariotti, L., Sylla, M. B., Bi, X., et al. (2012). RegCM4: Model description and preliminary tests over multi- ple CORDEX domains. *Climate Research*, *52*, 7–29. https://doi.org/10.3354/cr01018

22. Herrera-Lormendez, P., John, A., Douville, H., & Matschullat, J. (2023). Projected changes in synoptic circulations over Europe and their implications for summer precipitation: A CMIP6 perspective. *International Journal of Climatology*, 43(7), 3373–3390. https://doi.org/10.1002/joc.8033

23. IPCC (2021) Climate Change 2021: The Physical Science Basis. Contribution of Working Group I to the Sixth Assessment Report of the Intergovernmental Panel on Climate Change [Masson-Delmotte, V., P. Zhai, A. Pirani, et al.]. Cambridge University Press, Cambridge, United Kingdom and New York, NY, USA, In press, doi:10.1017/9781009157896

24. Kohonen T (2001) Self-Organizing Maps. Springer, New York.

25. Kirchmeier-Young MC, Zwiers FW, Gillett NP (2017) Attribution of extreme events in Arctic Sea ice extent. J Clim 30(2):553–571. https://doi.org/10.1175/JCLI-D-16-0412.1

26. Lehner F, Deser C, Maher N, et al. (2020) Partitioning climate projection uncertainty with multiple large ensembles and CMIP5/6. Earth Sys Dyn 11:491–508. doi:https://doi.org/10.5194/esd-11-491-2020

27. Maraun, D. and Widmann, M. (2018) Statistical Downscaling and Bias Correction for Climate Research. Cambridge: Cambridge University Press.

28. Martinez DM, Solman SA (2022) Synoptic patterns associated with extreme precipitation events over southeastern South America during spring and summer seasons. International Journal of Climatology, 1–20. https://doi.org/10.1002/joc.7911

29. Mueller WA et al (2018) A high-resolution version of the Max Planck Institute Earth System Model MPI-ESM1.2-HR. J Adv Model EarthSyst 10:1383–1413. doi:https://doi. org/10.1029/2017MS001217

30. Muñoz, Á. G., X. Yang, G. A. Vecchi, et al. 2017: A Weather-Type-Based Cross-Time-Scale Diagnostic Framework for Coupled Circulation Models. *J. Climate*, **30**, 8951–8972, https://doi.org/10.1175/JCLI-D-17-0115.1.

31. Nilsen, I., Fleig, A.K., Tallaksen, L.M., Hisdal, H., 2014. Recent Trends in Monthly Temperature and Precipitation Patterns in Europe. Hydrology in a Changing World: Environmental and Human Dimensions, vol. 363. IAHS Publ.

32. Olmo M, Bettolli ML, Rusticucci M (2020) Atmospheric circulation influence on temperature and precipitation individual and compound daily extreme events: spatial variability and trends over southern South America. Weather and Climate Extremes 29:100267 https://doi.org/10.1016/j.wace.2020.100267

33. Olmo ME, Bettolli ML (2021) Extreme daily precipitation in southern South America: Statistical characterization and circulation types using observational datasets and regional climate models. *Climate Dynamics*, *57*(3–4), 895–916. https://doi.org/10.1007/s00382-021-05748-2

34. Olmo, ME., Balmaceda-Huarte, R., Bettolli, ML. (2022) Multi-model ensemble of statistically downscaled GCMs over southeastern South America: historical evaluation and future projections of daily precipitation with focus on extremes. Climate Dynamics DOI: 10.1007/s00382-022-06236-x

35. Penalba OC, Robledo F (2010) Spatial and temporal variability of the frequency of extreme daily rainfall regime in the La Plata Basin during the 20th century. Clim Change 98(3):531–550

36. Pinto I, Jack C, Hewitson B (2018) Process-based model evaluation and projections over southern Africa from Coordinated Regional Climate Downscaling Experiment and Coupled Model Intercomparison Project Phase 5 models. International Journal of Climatology 1-11. DOI: 10.1002/joc.5666

37. Prein AF, Mearns LO (2021) U.S. Extreme precipitation weather types increased in frequency during the 20th century. *Journal of Geophysical Research: Atmospheres*, *126*, e2020JD034287. https://doi.org/10.1029/2020JD034287

38. Prein AF, Bukovsky MS, Mearns LO, et al. (2019) Simulating North American Weather Types With Regional Climate Models. *Front. Environ. Sci.* 7:36. doi: 10.3389/fenvs.2019.00036

39. Quagraine, KA., Hewitson, B., Jack, C., et al. (2020) Using co-behaviour analysis to interrogate the performance of CMIP5 GCMs over Southern Africa. J Clim 33:2891-2905.

40. Quintana JM, Aceituno P (2012) Changes in the rainfall regime along the extratropical west coast of South America (Chile): 30–43° S. Atmósfera 25(1):1–12

41. Robledo FA, Penalba OC, Bettolli ML (2013) Teleconnections between tropical-extratropical oceans and the daily intensity of extreme rainfall over Argentina. Int J Climatol 33(3):735–745. https://doi.org/10.1002/joc.3467

42. Salio P, Nicolini M, Zipser EJ (2007) Mesoscale convective systems over Southeastern South America and their relationship with the South American low level jet. Mon Weather Rev 135:1290–1309. https://doi.org/10.1175/MWR3305.1

43. Schuenemann KC, Cassano JJ (2010), Changes in synoptic weather patterns and Greenland precipitation in the 20th and 21st centuries: 2. Analysis of 21st century atmospheric changes using self-organizing maps, J. Geophys. Res., 115, D05108, doi:10.1029/2009JD011706.

44. Seager, R., Osborn, T.J., Kushnir, Y., Simpson, I.R., Nakamura, J. & Liu, H. (2019) Climate variability and change of Mediterranean-type climates. *Journal of Climate*, 32(10), 2887–2915. Available from: https://doi.org/10.1175/JCLI-D-18-0472.1

45. Stryhal, J., & Huth, R. (2018). Classifications of winter atmospheric circulation patterns: Validation of CMIP5 GCMs over Europe and the North Atlantic. Climate Dynamics, 52(5–6), 3575–3598. https://doi.org/10.1007/s00382-018-4344-7

46. Swart NC, Cole JNS, Kharin VV, et al. (2019) The Cana- dian earth system model version 5 (CanESM5.0.3). Geoscientific Model Development Discussions 5:1–68. https://doi.org/10.5194/

gmd-2019-177

47. Taylor KE (2001) Summarizing multiple aspects of model performance in a single diagram. J Geophys Res 106(D7):7183–7192.https://doi.org/10.1029/2000JD900719

48. Taylor KE, Stouffer RJ, Meehl GA (2012) An overview of CMIP5 and the experiment design. Bulletin of the American Meteorological Society, 93(4), 485–498. https://doi.org/10.1175/BAMS-D-11-00094.1

49. Varuolo-Clarke AM, Smerdon JE, Williams AP, Seager R (2021) Gross Discrepancies between Observed and Simulated Twentieth-to-Twenty-First-Cen´´tury Precipitation Trends in Southeastern South America. J Clim 34(15):6441–6457. https://doi.org/10.1175/JCLI-D-20-0746.1

50. Voldoire A, Sanchez-Gomez E, Salas y Mélia D, Decharme B, Cassou C et al (2013) The CNRM-CM5.1 global climate model: description and basic evaluation. Clim Dyn 40:2091–2121. DOI:https://doi.org/10.1007/s00382-011-1259-y

51. Volodin EM, Mortikov EV, Kostrykin SV, et al. (2017) Simulation of the present day climate with the climate model INMCM5. Clim Dyn V49:3715. https://doi.org/10.1007/s00382-017-3539-7

52. Wang, C., Soden, B. J., Yang, W., & Vecchi, G. A. (2021). Compensation between cloud feedback and aerosol-cloud interaction in CMIP6 models. *Geophysical Research Letters*, 48, e2020GL091024. https://doi.org/10.1029/2020GL091024

53. Wilks, D. S. (2019). Statistical methods in the atmospheric sciences (4th ed., p. 840). Elsevier.
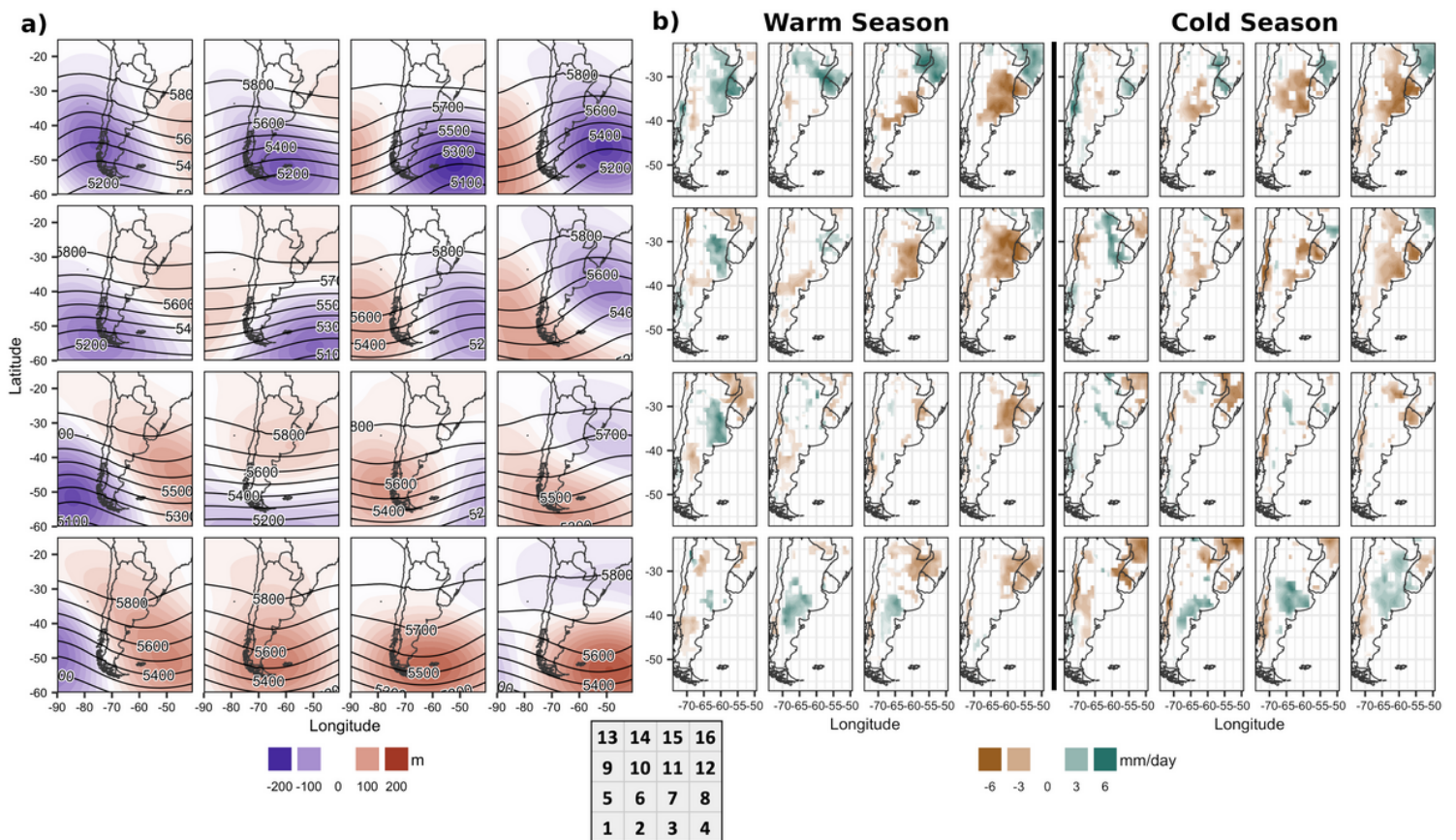
Figures

Figure 1

SOM classification over SSA, adapted from Olmo and Bettolli 2021: **a)** Z500 anomalies (raw) for each CP of the SOM in shaded (contours); **b)** Precipitation anomalies associated with each CP. Only significant anomalies are plotted (95% level of confidence). The bottom square shows the disposition and number of CPs in the SOM.
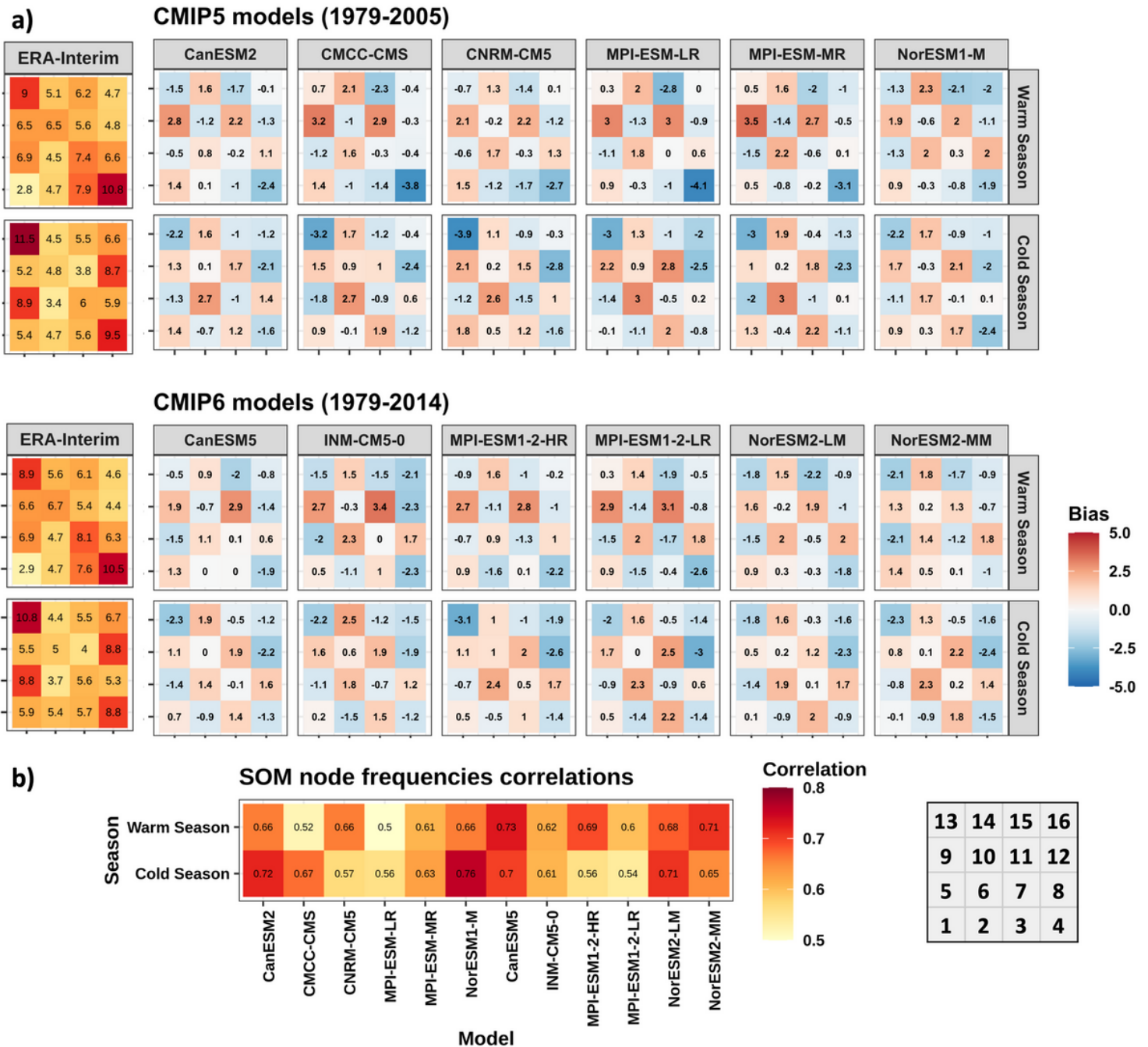

Figure 2

a) Heatmaps of node frequency difference (bias in percentage) along the SOM classification for each CMIP5 (first row) and CMIP6 (second row) GCM during their historical periods (1979-2005 and 1979-

2014, respectively) in the warm and cold seasons. ERA-Interim frequency of days along the SOM is shown for comprehensive purposes (first column); **b)** Pearson correlation between the observed SOM frequencies (ERA-Interim) and the GCM simulated ones. The bottom square shows the disposition and number of CPs in the SOM.
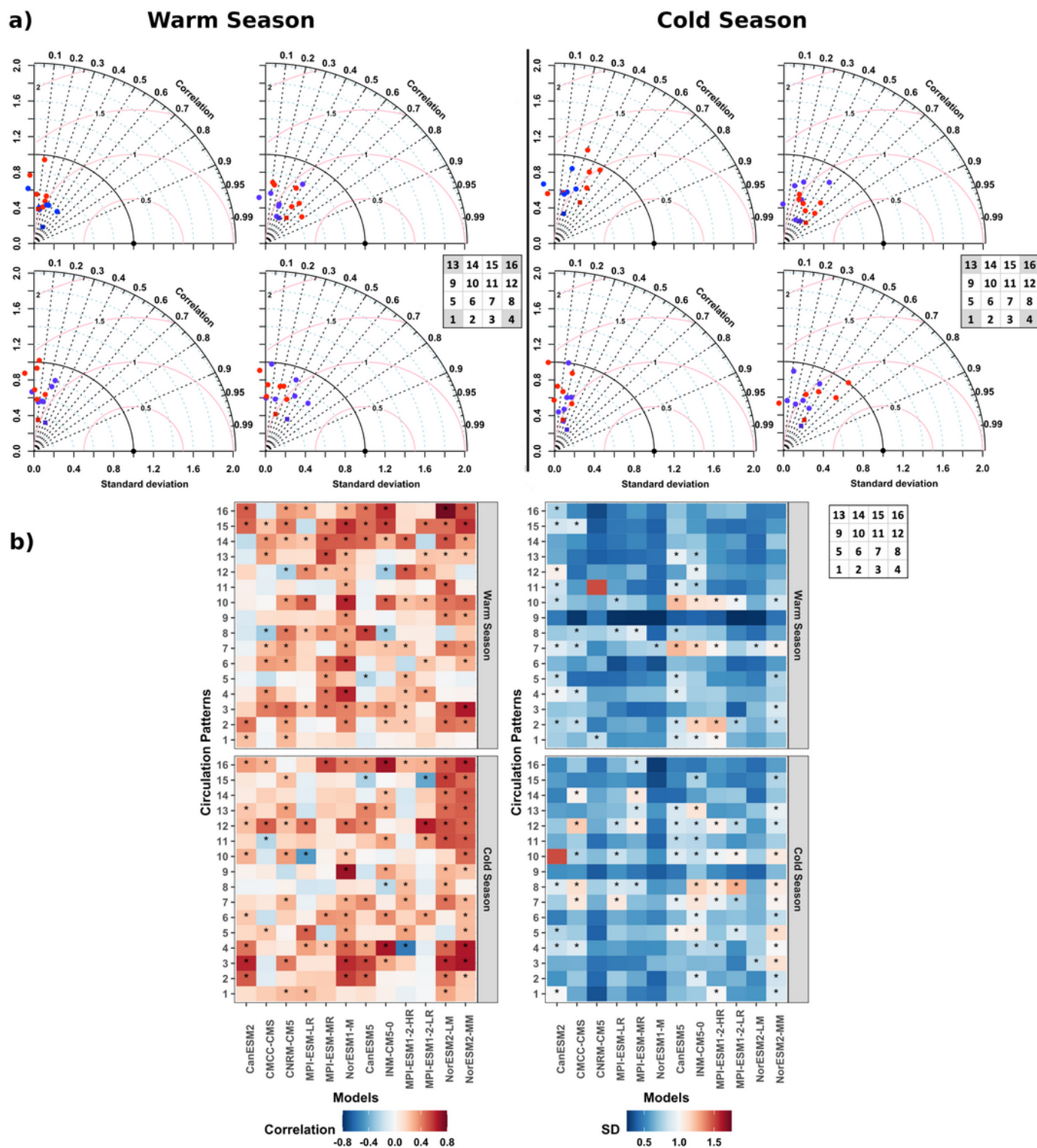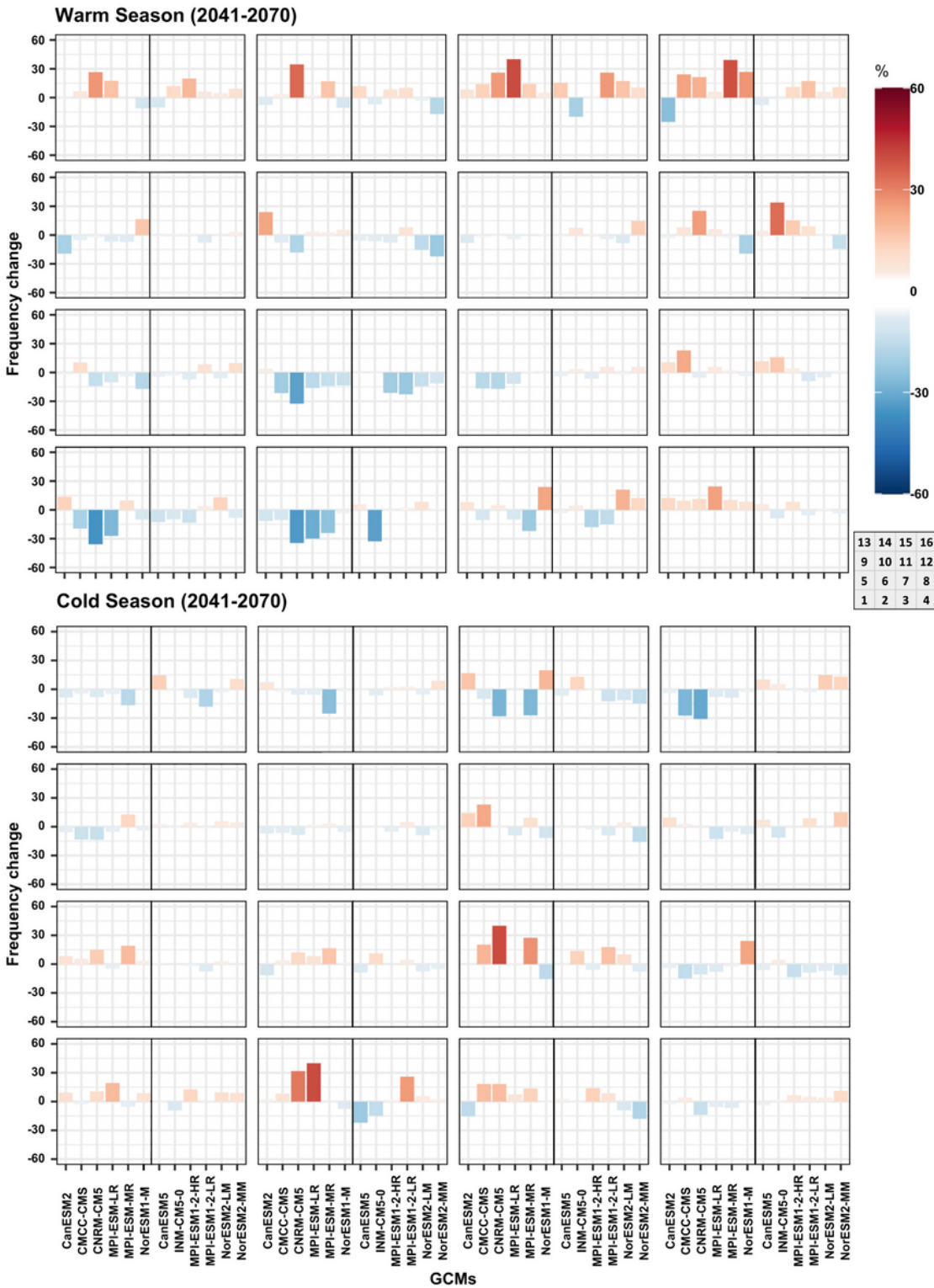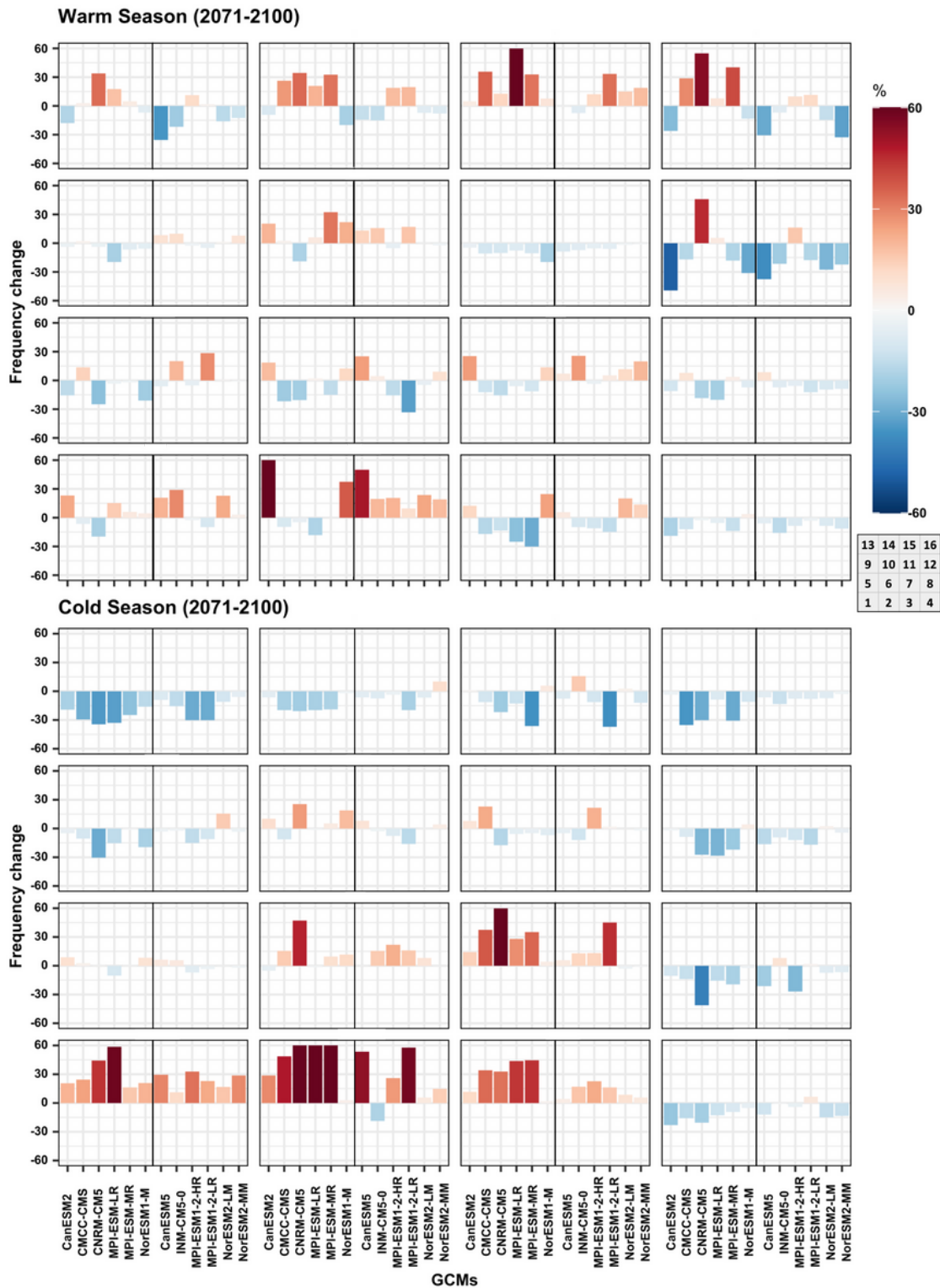

Figure 3

a) Taylor diagrams for the simulated rainfall patterns associated with the CPs located at the corners of the SOM for each GCM (CP1 and CP4 in the bottom rows and CP13 and CP16 in the top rows). Blue (red) points correspond to CMIP5 (CMIP6) individual models, whereas each experiment ensemble is presented with a filled square. Points outside the diagram correspond to negative spatial correlation values; **b)** Correlations and normalised standard deviation (SD) as shown in the Taylor diagrams but for all the 16 CPs in the SOM. Significant correlations and, for the SD, non-rejected equal variances (at the 95% level of confidence) are shown with an asterisk. The square shows the disposition and number of CPs in the SOM.
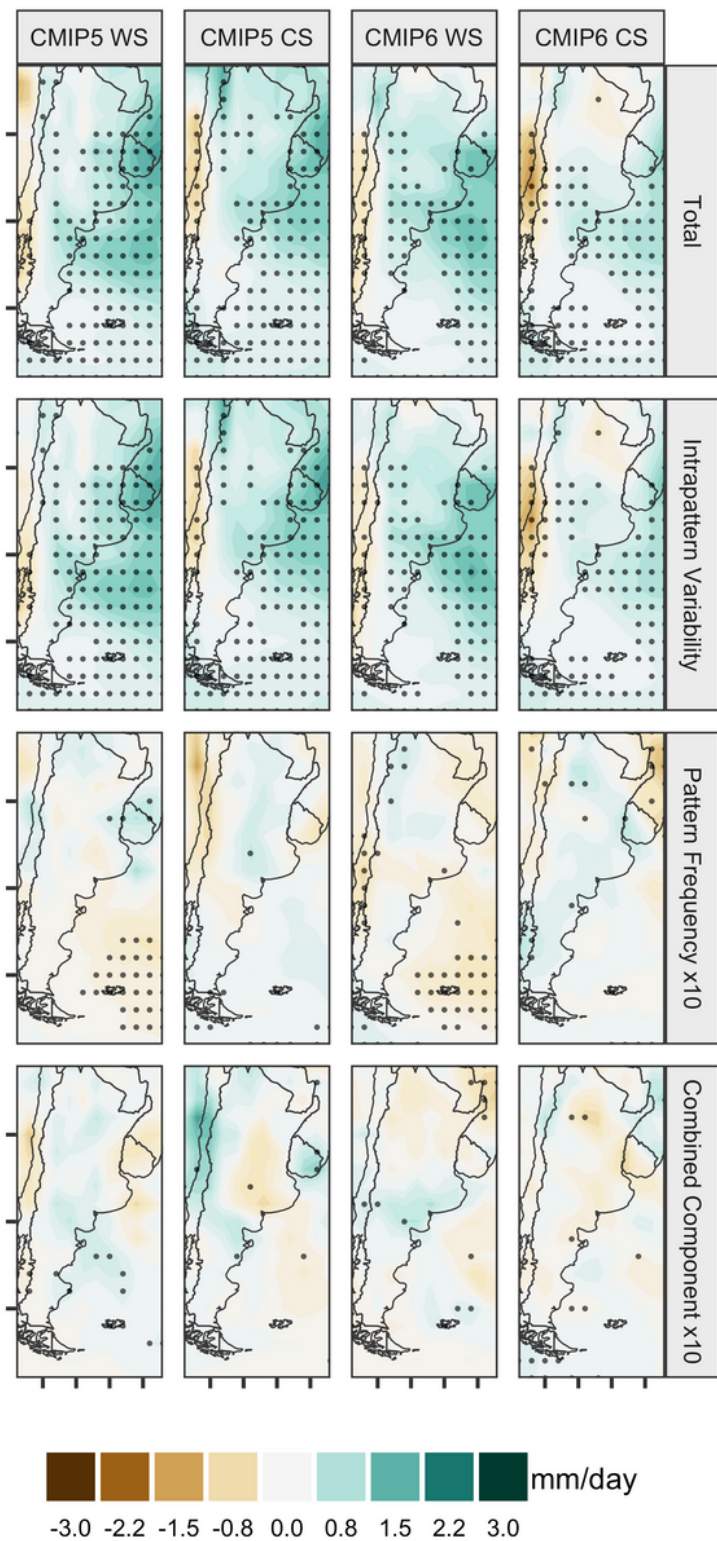
Figure 4

Changes in the frequency of the CPs for the near future (2041-2070) compared to the historical reference period 1986-2005. Each bar corresponds to a different GCM (from left to right, CMIP5 and CMIP6 models), considering the worst-case scenario in each CMIP experiment. The square below the colorbar shows the disposition and number of CPs in the SOM.

Figure 5

Same as Figure 4 but for the late future (2071-2100), considering the worst-case scenario in each CMIP experiment.

Figure 6

Attributional analysis for precipitation changes during the late future period 2071-2100 as depicted by the CMIP5 and CMIP6 model ensembles (the average of the changes of individual simulations for the worst-case scenario in each experiment) during the warm and cold seasons, separately. From top to bottom rows, rainfall changes compared to the historical periods due to: total precipitation; intrapattern variability

component; pattern frequency component and the combined (residual) component. Grid cells with significant changes in the model ensemble are shown with dots.

Supplementary Files

This is a list of supplementary files associated with this preprint. Click to download.

- SupplementaryMaterial.docx